Numerical study of circulation, dispersion, and hydrodynamic connectivity of surface waters on the Belize shelf

Liqun Tang,[1,2] Jinyu Sheng,[1] Bruce G. Hatcher,[1] and Peter F. Sale[3]

Received 23 February 2005; revised 8 June 2005; accepted 14 October 2005; published 12 January 2006.

[1] A nested grid ocean circulation modeling system is used to examine the circulation, dispersion, and hydrodynamic connectivity of surface waters on the Belizean shelf. The nested grid system consists of a coarse-resolution (~19 km) outer model of the western Caribbean Sea, an intermediate-resolution (~6 km) middle model of the southern Meso-American Barrier Reef System (MBRS), and a fine-resolution (~2 km) inner model of the Belizean shelf. The nested system is forced by climatological monthly mean surface forcing and integrated over 5 years. The near-surface circulation on the Belize shelf produced by the inner model is characterized by a strong and persistent northwestward flow as a direct influence of the Caribbean Current on the northwestern shelf and a weak and spatially variable flow on the inner and southern shelf. The monthly mean model currents are used to calculate retention and dispersion of conservative, near-surface particles carried by the ocean currents. The near-surface dispersion is relatively higher in areas seaward (east) of Lighthouse and Glovers Reef atolls and lower on the inner shelf, particularly within the Inner Channel and in the vicinity of South Water Cay. To examine hydrodynamic connectivity of reefs in the surface waters of the Belize shelf, we calculate upstream and downstream retention areas for coral reefs at Turneffe Islands and Glovers Reef atolls. The potential sources of passive, near-surface particle supply reaching these two reef atolls within 30 days include both the shallow waters surrounding the two sites, the deep waters between them, and the coastal waters of the Bay Islands (Honduras). The 30-day downstream retention areas of the Turneffe and Glovers Reef atolls cover the central and southern Belize shelf, respectively.

Citation: Tang, L., J. Sheng, B. G. Hatcher, and P. F. Sale (2006), Numerical study of circulation, dispersion, and hydrodynamic connectivity of surface waters on the Belize shelf, *J. Geophys. Res.*, *111*, C01003, doi:10.1029/2005JC002930.

1. Introduction

[2] The mechanisms and intensities of connection among populations and communities of organisms associated with geographically distinct coral reef structures (i.e., their habitats) are topics of intense research because of the apparent degradation of these charismatic ecosystems at the global scale [*Hughes and Tanner*, 2000; *Wilkinson*, 2004], and the trend toward spatially explicit, ecosystem-based management of coral reef provinces [*Gibson et al.*, 1998; *Lawrence et al.*, 2002]. Measuring connectivity in these well-bounded systems also contributes to emerging theory of marine metapopulation dynamics [*Palumbi*, 2003]. Of paramount relevance to understanding ecological connectivity is the interaction between physical and biological processes in exchanges of inorganic and organic materials among reef "islands" in deep water environments inimical to the sessile or site-attached stages of the life cycles of coral reef organisms. Most challenging of this research is predicting the trajectories of the immense diversity of living spores and larvae that provide an extended pelagic stage in the life histories of the majority of otherwise sedentary reef-associated species. Particular attention has been focused on connections among site-attached populations of coral reef fish, but models to date have used crude dynamics [*Roberts*, 1997] or have been restricted to small domains [*Cowen et al.*, 2000]. Our approach is to first differentiate, scale and parameterize the physical processes of advection and diffusion that affect the dispersion of bioparticles among reef units and model them at appropriate spatial-temporal scales; then to do the same for the biological processes of spawning release, development, directed locomotion, and settlement; and finally to combine the two model schema in a coupled, bio-physical model [*Hatcher et al.*, 2004]. Here we report on the first component of this endeavor we have undertaken in the Meso-American Barrier Reef System (MBRS) of the western Caribbean Sea (WCS).

[3] The Belize shelf (BS) in the northwest Caribbean Sea is a narrow, rugged continental shelf, bounded by the Central American continent to the west, Yucatan shelf to the north, Yucatan Basin to the east, and Gulf of Honduras to the south. The main topographic features in the vicinity

[1]Department of Oceanography, Dalhousie University, Halifax, Nova Scotia, Canada.
[2]Now at Department of Sedimentation Engineering, Institute of Water Resources and Hydropower Research, Beijing, China.
[3]Biological Science, University of Windsor, Windsor, Ontario, Canada.

0148-0227/06/2005JC002930$09.00

of the BS (Figure 1) are the Belize Barrier Reef (BBR) which, at 230 km length is the longest barrier reef system in the western Atlantic; three large off-shelf atolls known as Lighthouse Reef Atoll (LRA), Turneffe Islands Atoll (TIA) and Glovers Reef Atoll (GRA); and numerous patch reefs across the shelf [*Purdy*, 1974; *MacIntyre and Aronson*, 1997; *Kramer and Kramer*, 2002].

[4] Reef ecosystems are the marine equivalents of terrestrial rainforests in terms of biodiversity [*Hubbell*, 1997], and have significant economic values in terms of exploited resources, waste disposal, protection of coastal property and as a basis for tourism [*Cesar*, 2000; *de Groot et al.*, 2002]. The coral reefs and associated lagoons on the BS serve as important habitat, breeding and feeding grounds for a great diversity of marine invertebrates, fish, reptiles and mammals. Many sites known to be used by reef fish spawning aggregations occur throughout the MBRS [*Sadovy and Vincent*, 2002], and there are some fifteen marine protected areas in the region [*Kramer and Kramer*, 2002]. Establishing the source-sink relationships among reef areas will inform the prioritization of protective management interventions. Reefs of the BS have also been affected significantly by natural and anthropogenic factors including hurricanes, disease outbreaks, coral bleaching and various disturbances and stresses resulting from human activities in the region over the last 30 years [*Gibson et al.*, 1998; *Williams and Bunkley-Williams*, 2000]. *Aronson et al.* [2000] demonstrated that the mass mortality of acroporid corals in the region during the late 1990s was unprecedented over the last 3000 years. There is thus an increasing demand for better understanding of physical, ecological and biological processes that connect and sustain the marine ecosystems of the BS and the broader Caribbean. The lack of robust, fine-scale models of circulation and hydrodynamic dispersion in the MBRS poses a serious impediment to meeting this demand.

[5] Circulation, dispersion and connectivity among coral reefs have been studied using various numerical models of systems at a wide range of scales. The Caribbean Sea eddies have been analyzed and simulated using a sea level data of the TOPEX/Poseidon altimeter and a (1/6)° Atlantic Ocean model [*Carton and Chao*, 1999]. The seasonal circulation, larval dispersal and retention in the Caribbean Sea were examined by *Cowen et al.* [2003] using a (1/12)° North Atlantic Ocean model constructed from the Miami Isopycnic Coordinate Ocean Model (MICOM). The most comprehensive modeling and empirical work linking physical and biological aspects has been done for Australia's Great Barrier Reef (GBR) on the North Queensland Shelf [*Andrews et al.*, 1983; *Wolanski et al.*, 2001, and references therein]. Eddy-resolving numerical models have been used to simulate three-dimensional (3D) circulation and dispersal of material, such as larvae of marine organisms, on a reef in the central GBR [*Black*, 1993], and to discriminate between local trapping (i.e., retention) of neutrally buoyant, passive material coming from a natal reef versus trapping of this material on reefs downstream [*Black et al.*, 1991]. Most other modeling studies have also focused at the reef to subreef scales (at length scales of 1 to 0.01 km). For example, *Hearn et al.* [2001] used a numerical model of a set of platform reefs on the Western Australian shelf to compare hydrodynamic connectivity among island sites

Figure 1. Topographic map of the Belizean shelf modified from the map constructed by Casado Internet Group.

with the genetic connectivity among subpopulations of marine gastropods at these sites.

[6] Typically, models of this type are scaled to capture the local dynamics of water around topographically complex reef structures, and computational limitations restrict the model domain to small portions of the potential advective ambit of bioparticles that live for weeks or months in the water column before settling to reef substrata. For predictions over larger domains, models of reef connectivity in the Caribbean Sea have used coarse-resolution depictions of current patterns that do not resolve realistic dynamics and circulation patterns around source and sink reefs [e.g., *Roberts*, 1997; *Cowen et al.*, 2000]. The challenge at this stage is to develop models that hydrodynamically connect individual reef units across distances that incorporate realistic marine dispersal domains, while retaining the fine-scale resolution of the hydrodynamic processes around reefs that influence key ecological processes of dispersal, retention and settlement.

[7] In this paper we present a three-level nested grid, three-dimensional ocean circulation modeling system designed to deal with the resolution domain challenge. The nested system is used to study the upper ocean circulation on the BS and examine the hydrodynamic dispersion and connectivity in surface waters on the basis of the horizontal movements of near-surface particles that

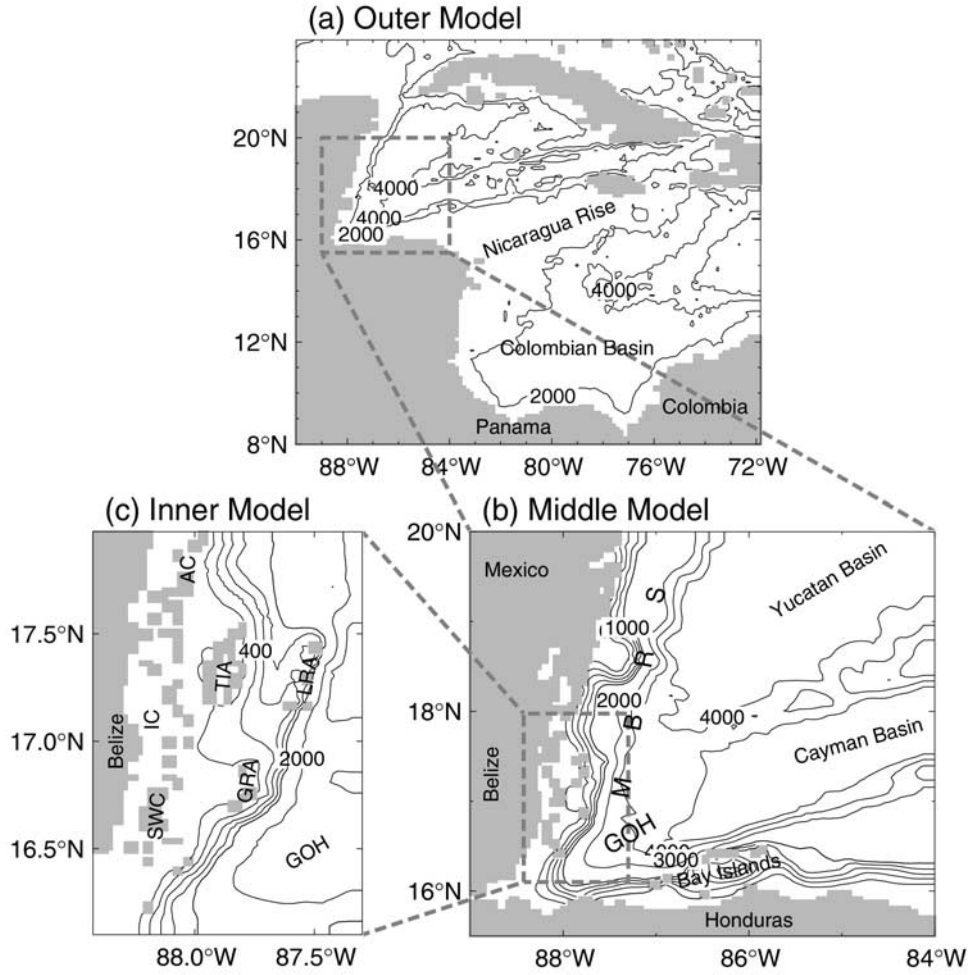

Figure 2. Selected bathymetric features for the triply nested grid modeling system, which consists of (a) an outer model covering western Caribbean Sea (WCS), (b) a middle model covering the southern Meso-American Barrier Reef System (MBRS), and (c) an inner model covering the Belizean shelf (BS). Abbreviations are used for Lighthouse Reef Atoll (LRA), Turneffe Islands Atoll (TIA), Glovers Reef Atoll (GRA), South Water Cay (SWC), Inner Channel (IC), and Ambergris Cay (AC). Contours are labeled in units of meters.

are advected passively by the model currents among the three nested model domains of increasing spatial resolution. We first describe the nested grid system and the two-way nesting technique on the basis of the smoothed semiprognostic method [*Greatbatch et al.*, 2004; *Sheng et al.*, 2005b]. We then present the annual mean and monthly mean circulations in the upper ocean of the BS, the horizontal movements of passive particles in the near-surface layer, and metrics of the hydrodynamic dispersion and connectivity of surface waters on the BS.

2. Nested Grid Ocean Circulation Modeling System

2.1. Ocean Circulation Model

[8] The nested grid ocean circulation modeling system used in this study is based on the primitive equation, three-dimensional ocean circulation model known as CANDIE (Canadian version of DieCAST [*Sheng et al.*, 1998]). CANDIE is an outgrowth of the DieCAST model developed by *Dietrich et al.* [1987] and has been successfully applied to various modeling problems on the continental shelf, including wind-driven circulation over an idealized coastal canyon [*Sheng et al.*, 1998], nonlinear dynamics of a density-driven coastal current [*Sheng*, 2001], tidal circulation in the Gulf of St. Lawrence [*Lu et al.*, 2001] and wind-driven circulation over a stratified coastal embayment [*Davidson et al.*, 2001]. Most recently, CANDIE has been used to study the storm-induced circulation on the Scotian Shelf [*Sheng et al.*, 2005a], seasonal circulation in the western Caribbean Sea [*Sheng and Tang*, 2003, 2004], and nonlinear tidal circulation in coastal waters [*Sheng and Wang*, 2004].

[9] The nested grid modeling system has a three-level nesting structure (Figure 2), which consists of an outer model covering the WCS (72°–90°W, 8°–24°N), a middle model covering the southern MBRS (84°–89°W, 15.5°–20°N), and an inner model covering the BS (87.3°–88.43°W, 16.1°–18°N). The nested grid modeling system uses different time steps for the three subcomponents, which are 16 minutes for the outer model, 5.5 minutes for the middle model and 2 minutes for the inner model. The nested

system uses the digital bathymetry database of 2-minute resolution (DBDB2) developed by the Ocean Dynamics and Prediction Branch, the Naval Research Laboratory of the United States (D.-S. Ko, personal communication, 2003; http:/www7320.nrlssc.navy.mil/DBDB2_WWW). The horizontal resolutions of the nested system are approximately 19 km for the outer model, 6 km for the middle model, and 2 km for the inner model, respectively. The three subcomponents of the nested system have the same 31 unevenly spaced z levels with the centers of each level located at 5, 16, 29, 44, 61, 80, 102, 128, 157, 191, 229, 273, 324, 383, 450, 527, 615, 717, 833, 967, 1121, 1297, 1500, 1733, 2000, 2307, 2659, 3063, 3528, 4061, and 4673 m, respectively. For simplicity, model grid points with water depth less than 5 m are treated as land (dry) points. Due mainly to their coarse horizontal resolutions, the outer and middle models of the nested system resolve reasonably well the large-scale features (Figures 2a and 2b), but less well small-scale features of real topography on the BS. In comparison, the inner model resolves better the three large reef atolls LRA, TA, and GRI (Figure 2c), but less well the coastal topography and patch reefs on the BS.

[10] The nested system uses the vertical mixing scheme of *Large et al.* [1994] for vertical eddy viscosity and diffusivity coefficients K_m and K_h, and the horizontal mixing scheme of *Smagorinsky* [1963] for the horizontal eddy viscosity coefficient A_m defined as

$$A_m = c\Delta x\Delta y\sqrt{\left(\frac{\partial u}{\partial x}-\frac{\partial v}{\partial y}\right)^2+\left(\frac{\partial u}{\partial y}+\frac{\partial v}{\partial x}\right)^2} \quad (1)$$

where Δx and Δy are the grid spacing in the eastward and northward directions, respectively, u and v are the eastward and northward components of model currents, respectively, and c is a coefficient set to 0.1. The horizontal turbulent Prandtl Number A_h/A_m is set to 0.1., where A_h is the horizontal eddy diffusivity coefficient. Since the Smagorinsky scheme is resolution-dependent, it has the desirable effect of having different levels of horizontal mixing in the different subcomponents of the nested system. The nested system also uses the fourth-order numerics [*Dietrich*, 1997] and Thuburn's flux limiter to discretize the nonlinear advection terms [*Thuburn*, 1996].

[11] The following model boundary conditions are used in the three subcomponents of the nested system. At lateral solid (or closed) boundaries, the normal flow, tangential stress of the currents and horizontal fluxes of temperature and salinity are set to zero (free-slip conditions). Along open boundaries of each subcomponent, the normal flow, temperature and salinity fields are calculated using adaptive open boundary conditions [*Marchesiello et al.*, 2001]. It first uses an explicit Orlanski radiation condition [*Orlanski*, 1976] to determine whether the open boundary is passive (outward propagation) or active (inward propagation). If the open boundary is passive, the model prognostic variables are radiated outward to allow any perturbation generated inside the model domain to propagate outward as freely as possible. If the open boundary is active, the outer model prognostic variables at the open boundary are restored to the monthly mean climatologies with a restoring timescale of 15 days, and the middle and inner model prognostic variables at the open boundary are restored to the outer and middle model results, respectively, with a restoring timescale of 5 hours. In addition, the depth-mean normal flows across the outer model open boundaries are set to be the monthly mean results produced by a $(1/3)^\circ$ Atlantic model (C. Eden, personal communication, 2003) on the basis of FLAME (Family of Linked Atlantic Model Experiments [*Dengg et al.*, 1999]).

2.2. Two-Way Nesting Technique Based on the Smoothed Semiprognostic Method

[12] The novel feature of the nested grid modeling system for the BS is the use of a two-way nesting technique based on the smoothed semiprognostic (SSP) method [*Sheng et al.*, 2005b]. The SSP method [*Eden et al.*, 2004] is a modification of the original semiprognostic (OSP) method introduced by *Sheng et al.* [2001]. The original application of both SSP and OSP methods was to adjust an ocean circulation model to correct for systematic error by adding a correction term to the model hydrostatic equation, which is equivalent to adding a pressure correction term to the horizontal momentum equation. Readers are referred to *Greatbatch et al.* [2004] and *Sheng et al.* [2005b] for a detailed discussion on the SSP method and its application to the development of the new two-way nesting technique. Only a brief summary is provided here.

[13] The new nesting technique has two components: (i) the specification of the model's open boundary conditions described in 2.1 above, and (ii) the use of the SSP method to exchange information between subcomponents of the nested grid modeling system. Three steps are involved for the second component. First, the middle model temperature and salinity (TS) are interpolated onto the inner model grid to adjust the momentum equation of the inner model over the common subregion where the inner and middle model grids overlap on the basis of

$$\frac{\partial p_{inn}}{\partial z} = -g\rho_{inn} - g(1-\beta_{inn})\langle\hat{\rho}_{mid} - \rho_{inn}\rangle \quad (2)$$

where p_{inn} and ρ_{inn} are pressure and density variables of the inner model, respectively, $\hat{\rho}_{mid}$ is density calculated from the middle model TS fields after interpolation onto the inner model grid, β_{inn} is the linear combination coefficient with a value between 0 and 1, and $\langle\rangle$ is a filtering operator. The filtering operator ensures that the inner model is constrained by the middle model only on large scales (determined by the smoothing scale that is used), the smaller scales associated with the fine grid of the inner model being free to evolve without constraint.

[14] Second, the middle model TS fields are interpolated onto the outer model grid to adjust the momentum equations of the outer model over the common subregion where the outer and middle model grids overlap on the basis of

$$\frac{\partial p_{out}}{\partial z} = -g\rho_{out} - g(1-\beta_{out})\langle\tilde{\rho}_{mid} - \rho_{out}\rangle \quad (3)$$

where p_{out} and ρ_{out} are pressure and density variables of the outer model, respectively, $\tilde{\rho}_{mid}$ is density calculated from middle model TS fields after interpolation onto the outer model grid, β_{out} is the linear combination coefficient with a

value between 0 and 1, and $\langle\rangle$ is the filtering operator, which usually differs from that in equation (2).

[15] Third, the outer and inner model TS fields are interpolated onto the middle model grid to adjust the momentum equation of the middle model over the overlapping subregion on the basis of

$$\frac{\partial p_{mid}}{\partial z} = -g\rho_{mid} - g(1-\beta_{mid})\left\langle \hat{\rho}_{opi} - \rho_{mid} \right\rangle \tag{4}$$

where p_{mid} and ρ_{mid} are pressure and density variables of the middle model, respectively, $\hat{\rho}_{opi}$ is density calculated from the outer and inner model TS fields after interpolation onto the middle model grid, and β_{mid} is the linear combination coefficient with a value between 0 and 1.

[16] As demonstrated by *Sheng et al.* [2005b], the above SSP nesting technique is equivalent to adding an interaction term to the model momentum equation in each subcomponent of the nested system. The interaction term depends on the density difference between subcomponents of the nested system shown in the second terms in equations (2)–(4), with linear coefficients β_{inn}, β_{out} and β_{mid} determining the intensity of the interaction. When $\beta_{inn} = 1$, the inner model is not constrained by the middle model except for the specification of inner model boundary conditions based on the middle model results. Similarly, the outer model in the overlapping subregion is not constrained by the middle model when $\beta_{out} = 1$, and the middle model in the overlapping subregion is not constrained by the inner and outer models when $\beta_{mid} = 1$. In this study, we follow *Sheng et al.* [2005b] and set the linear combination coefficients β_{inn}, β_{out} and β_{mid} to 0.5. For simplicity the filtering operator used in this study is the running averaging, with a smoothing scale of 24 km for the inner model, and 72 km for the middle model. The filtering operator in equation (3) for the outer model is not used in this study.

[17] To correct for model systematic error and unsolved processes in the outer and middle models, the SSP nesting technique described above is also combined with the original application of the SSP method. The combination is achieved by replacing $\tilde{\rho}_{mid}$ in equation (3) with $\alpha_{out}\,\tilde{\rho}_{mid} + (1-\alpha_{out})\,\rho_c$ for the outer model, where ρ_c is the climatological density and α_{out} is set to 0.5, and replacing $\hat{\rho}_{opi}$ in equation (4) by $\alpha_{mid}\,\hat{\rho}_{opi} + (1-\alpha_{mid})\,\rho_c$, with α_{mid} set to 0.25 for the middle model. The reader is referred to *Sheng et al.* [2005b] for a more detailed discussion on this combination.

2.3. Model Forcing and Trajectory Tracking of Passive Particles

[18] The nested grid modeling system is initialized with January mean climatology of temperature and salinity (TS), and forced by the climatological monthly mean surface wind stress and heat flux constructed by *da Silva et al.* [1994]. The net heat flux through the sea surface Q_{net} is expressed as [*Barnier et al.*, 1995]:

$$Q_{net} = Q_{net}^{clim} + \gamma\left(SST^{clim} - SST^{\text{model}}\right) \tag{5}$$

where Q_{net}^{clim} is the monthly mean net heat flux taken from *da Silva et al.* [1994], SST^{clim} is the monthly mean sea surface temperature, and γ is the coupling coefficient defined as $\Delta z_1\,\rho_0\,c_p/\tau_Q$, where Δz_1 is the thickness of the top z level, c_p is the specific heat, and τ_Q is the restoring timescale which is set to 15 days. The implied value of γ is about 35 $Wm^{-2}\ K^{-1}$, which is comparable to values calculated from observations [e.g., *Haney*, 1971]. We also restore the model sea surface salinity to the monthly mean climatology at a timescale of 15 days. Since the model forcing in this study is the monthly mean climatology, it is sufficient to exchange information between the subcomponents of the nested system once per day.

[19] To examine the dispersion and connectivity of surface waters in the BS, we track the movements of near-surface particles that are advected passively by horizontal components of ocean currents (by ignoring vertical movements of particles) on the basis of

$$\vec{x}(t) = \vec{x}(t_0) + \int_{t_0}^{t} \vec{u}(\vec{x}, t)dt + \vec{\delta} \tag{6}$$

where $\vec{x}\,(t)$ and $\vec{x}(t_0)$ are the horizontal position vectors of a passive particle at time t and initial time t_0, respectively, $\vec{u}(\vec{x}, t)$ is the horizontal velocity vector of model currents, and $\vec{\delta}$ is additional random horizontal displacements used to represent the influence of physical processes such as storm events, daily wind forcing and tidal currents that are not modeled explicitly in this study. Justification for ignoring the vertical movements of particles in equation (6) is that monthly mean horizontal currents are on average much stronger than the vertical currents in the study region in the surface layer of the BS.

[20] We follow *Hannah et al.* [1998] and express $\vec{\delta}$ as

$$\vec{\delta} = \left(\xi\sqrt{2\kappa\Delta t}, \varsigma\sqrt{2\kappa\Delta t}\right) \tag{7}$$

where ξ and ζ are random deviates from a Gaussian distribution of zero mean and unit variance, respectively, Δt is the time step used in the numerical integration of equation (6), which is greater than the time steps used in the numerical simulation of the nested grid modeling system, and κ is a horizontal eddy diffusivity set to 25 m^2s^{-1} [*Hannah et al.*, 1998].

[21] To quantify retention and dispersion of passive particles (i.e., conservative with respect to the water mass), we follow *Cong et al.* [1996] and define the retention index as

$$R(\vec{x}, t) = \frac{N(\vec{x}, t)}{N(\vec{x}, t_0)} \tag{8}$$

where $N(\vec{x}, t_0)$ is the number of particles inserted initially in a subarea of a given size centered at $\vec{x}$ at initial time t_0, and $N(\vec{x}, t)$ is the number of original particles remaining within the subarea at some later time t. Physically, the retention index defined above represents the proportion of particles inserted in a given subarea at t_0 remaining inside the subarea at a later time t. The value of R is between 0 and 1, with higher values corresponding to higher retention of particles. In the case of $R = 0$, all the particles are flushed from the given subarea between time t_0 and t. Once the retention index R is known, the dispersion rate can readily be calculated on the basis of $1 - R(\vec{x}, t)$. Therefore we focus

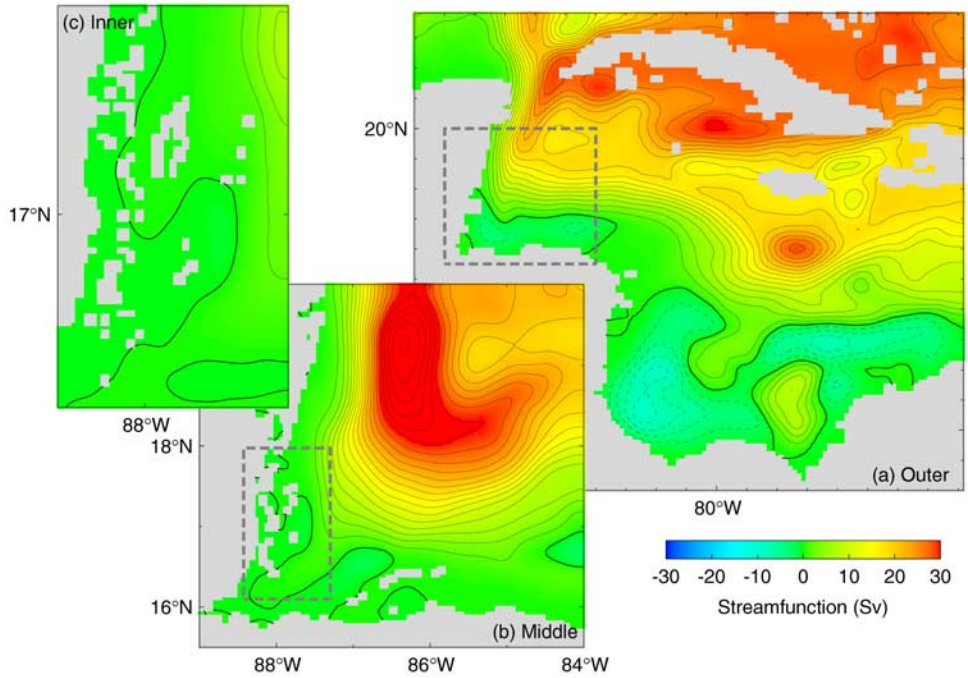

Figure 3. Annual mean volume transport stream function calculated from 4-year model results. The contour interval is 2 Sv (=10^6 m^3 s^{-1}).

mainly on the calculation and discussion of the retention index in this study.

3. Model Results

3.1. Annual and Monthly Mean Upper Ocean Circulation

[22] We integrate the nested grid system for 5 years and calculate the annual mean volume transport streamfunction (Figure 3) from model results in the last 4 years. The large-scale features of the annual mean transport streamfunction produced by the outer model compare very well with the numerical results produced by *Smith et al.* [2000] and *Johns et al.* [2002] for the western Caribbean Sea (WCS). The annual mean transport of the Caribbean Current is about 18 Sv (=10^6 m^3 s^{-1}) over the eastern Colombian Basin, and increases gradually up to 22 Sv as flowing onto the western Yucatan Basin. The westward flow through the Windward Passage has a time-mean transport of about 7 Sv. The northward transport through the Yucatan Strait is about 25 Sv. All of the above mean transport values are consistent with the current knowledge of the mean transport in the region [*Murphy et al.*, 1999; *Johns et al.*, 2002; *Ezer et al.*, 2003].

[23] The annual mean, near-surface (5 m) circulation in the WCS produced by the coarse-resolution outer model is characterized by a persistent throughflow known as the Caribbean Current, which is relatively broad and roughly westward in the central and eastern Colombian Basin (Figure 4a). The Caribbean Current bifurcates before reaching the Nicaragua Rise, with a weak branch veering southwestward to form the cyclonic, highly variable Panama-Colombia Gyre in the southwestern Caribbean Sea. The main branch of the Caribbean Current turns northwestward and flows along the outer flank of Nicaragua Rise to form a narrow offshore flow running westward and then northward to the Gulf of Mexico. The main features of the annual mean circulation produced by the outer model are in good agreement with those produced by *Sheng and Tang* [2003] using a single-domain model for the same region, and are also in good agreement with the current knowledge of the general circulation in the WCS [*Maul*, 1993; *Mooers and Maul*, 1998; *Johns et al.*, 2002; *Ezer et al.*, 2003].

[24] The annual mean near-surface circulation produced by the middle model (Figure 4b) is dominated by the Caribbean Current that prevails in the southern MBRS. The Caribbean Current in this subregion runs first westward in the deep water off the continental shelf of Honduras, and then turns northward as it approaches the Gulf of Honduras (GOH) to form an intense coastal jet running northward along the east coast of Belize and Mexico.

[25] By comparison with the outer and middle model results in the BS, the fine-resolution inner model generates more mesoscale circulation features around individual reef structures in the same region (Figure 4c). In the area seaward (east) of Lighthouse Reef Atoll (LRA) and Turneffe Islands Atoll (TIA), the annual mean near-surface currents produced by the inner model are strong and approximately northwestward, as a direct influence of the Caribbean Current in these areas. The near-surface currents separate into two branches before reaching the southeastern margin of TIA, with the main branch veering anticyclonically to flow northward to the deep waters of the Belize barrier reef (BBR), and a weak branch flowing around the south tip of TIA before turning northward through a narrow passage between TIA and the BBR. The annual mean currents are relatively weak and spatially variable within the Inner Channel (IC) and in reef areas off Glovers Reef Atoll (GRA) and South Water Cay (SWC).

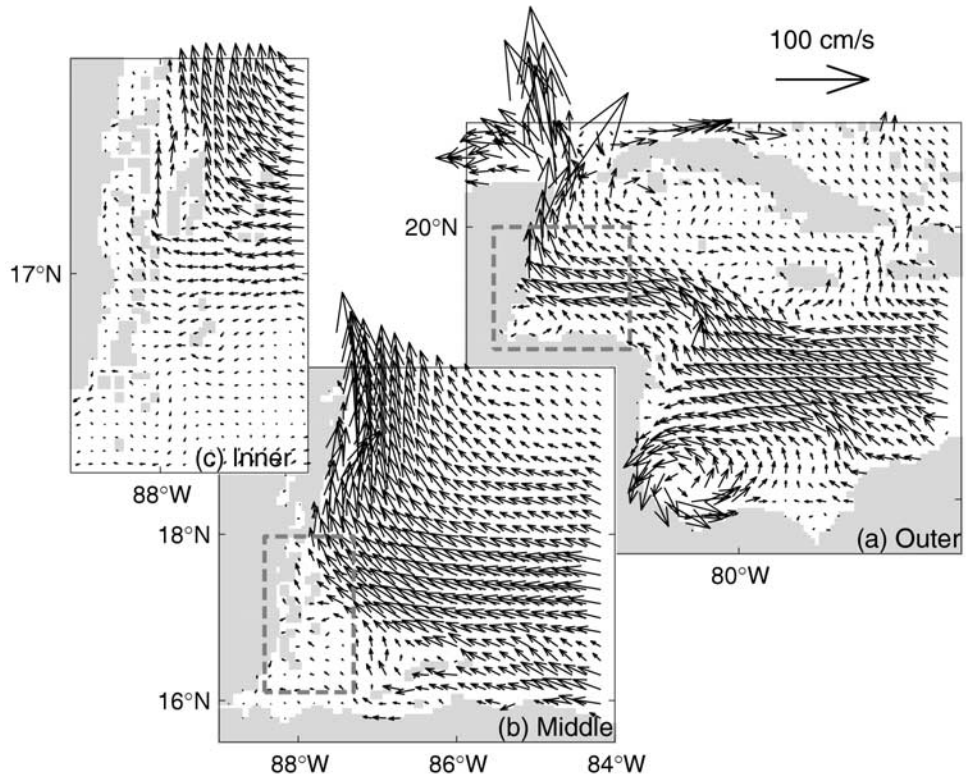

Figure 4. Annual mean near-surface (5 m) currents calculated from 4-year model results produced by the nested grid modeling system. Velocity vectors are plotted at every third model grid point.

[26] Figure 5 shows vertical distributions of the annual mean along-channel currents and temperature across Yucatan Strait produced by the outer model. The model results are in qualitative agreement with previous observations [*Maul et al.*, 1985; *Ochoa et al.*, 2001; *Sheinbaum et al.*, 2002] and numerical simulations [*Ezer et al.*, 2003; *Oey and Ezer*, 2004] in the strait, which are characterized as the surface-intensified Yucatan Current flowing into the Gulf of Mexico from the Caribbean Sea in the upper layer, weak Yucatan Countercurrent flowing southward beneath it over

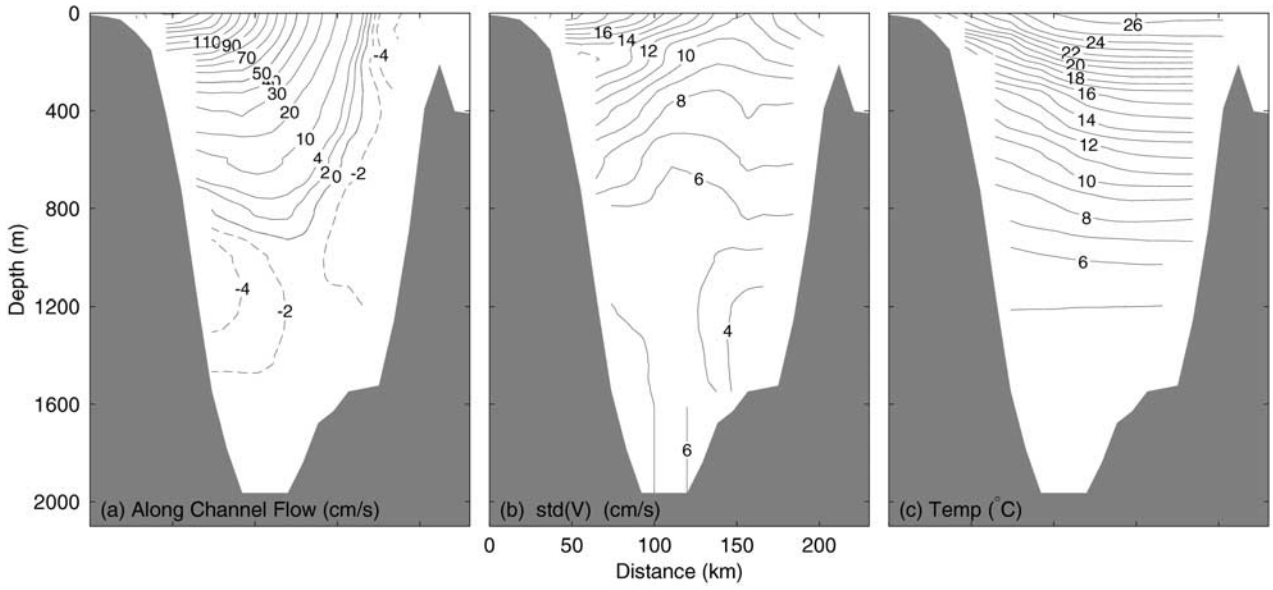

Figure 5. Vertical distributions of (a) along-channel (northward) annual mean currents, (b) associated standard deviations, and (c) annual mean temperature across Yucatan Strait calculated from 4-year model results produced by the nested grid outer model.

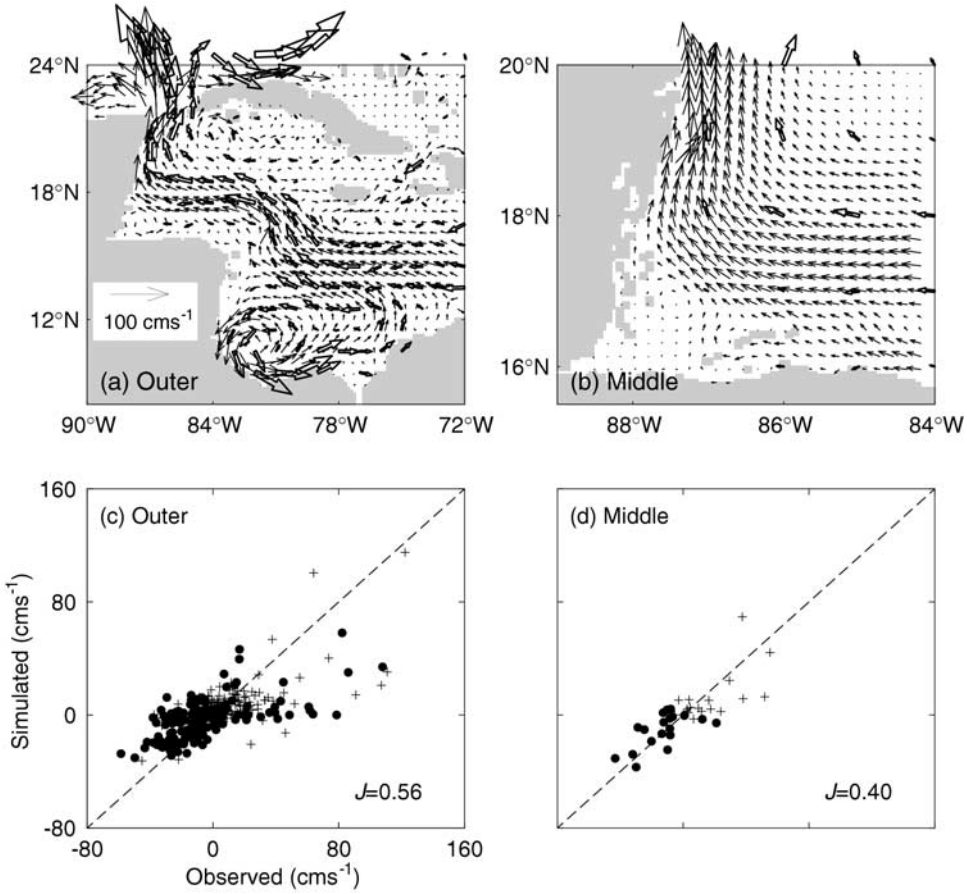

Figure 6. Comparison of modeled (solid arrows) and observed (open arrows) currents (a) in the western Caribbean Sea (WCS) and (b) in the southern Meso-American Barrier Reef System (MBRS). The modeled currents in the WCS and southern MBRS are the annual mean currents at 16 m produced by the nested grid outer and middle models, respectively. The observed currents are the gridded time-mean currents during the 1990s inferred from trajectories of 15-m-drogued satellite-tracked drifters by *Fratantoni* [2001] on a 1° grid. Scatterplots of observed and model-calculated time-mean currents (c) in the WCS and (d) in the southern MBRS.

the western side of the Strait, and southward flows at the surface and at depth on the Cuban side (Figure 5a). The annual mean temperature has the upward curvature of the isotherms in the top 500 m associated with the northward Yucatan Current in the Mexican side (Figure 5c). The change in curvature of the isotherms in the deep layer of greater than 800 m is associated with the Yucatan Countercurrents in the western side and Cuban Countercurrent in the eastern side [*Sheinbaum et al.*, 2002]. It should be noted that the model-calculated Yucatan Current is relatively stronger in the surface layer and the model-calculated Yucatan Countercurrent is slightly weaker than the observations made by *Sheinbaum et al.* [2002] on the western side of the Strait.

[27] We next follow *Sheng and Tang* [2003, 2004] and assess the performance of the nested system by comparing the annual mean currents at 16 m produced by the outer and middle models with the time-mean currents inferred by *Fratantoni* [2001] from trajectories of the satellite-tracked 15-m-drogued drifters made during the 1990s (Figure 6). The results of the nested grid outer model reproduce reasonably well the large-scale features of the observed currents in the WCS, including the persistent, Caribbean Current throughflow and the intense Panama-Colombia Gyre (Figure 6a). The middle model results also reproduce reasonably well the observed currents in the southern MBRS.

[28] To quantify the model performance, we calculate the misfit between the empirical observations and the model-computed currents on the basis of J, defined as:

$$J = \frac{\sum_{k}^{N} \left[\left(u_k^o - u_k^s\right)^2 + \left(v_k^o - v_k^s\right)^2 \right]}{\sum_{k}^{N} \left[\left(u_k^o\right)^2 + \left(v_k^o\right)^2 \right]} \tag{9}$$

where (u_k^o, v_k^o) are the horizontal components of the observed currents at the kth location estimated by *Fratantoni* [2001], (u_k^s, v_k^s) are the horizontal components of the simulated currents produced by the outer or middle models at the same kth location as the observations, respectively, and N is the total number of locations where observations were made. The smaller J, the better the model results fit the observations. The J value is about 0.54 for the outer model results in the WCS (see Figure 6c), and about

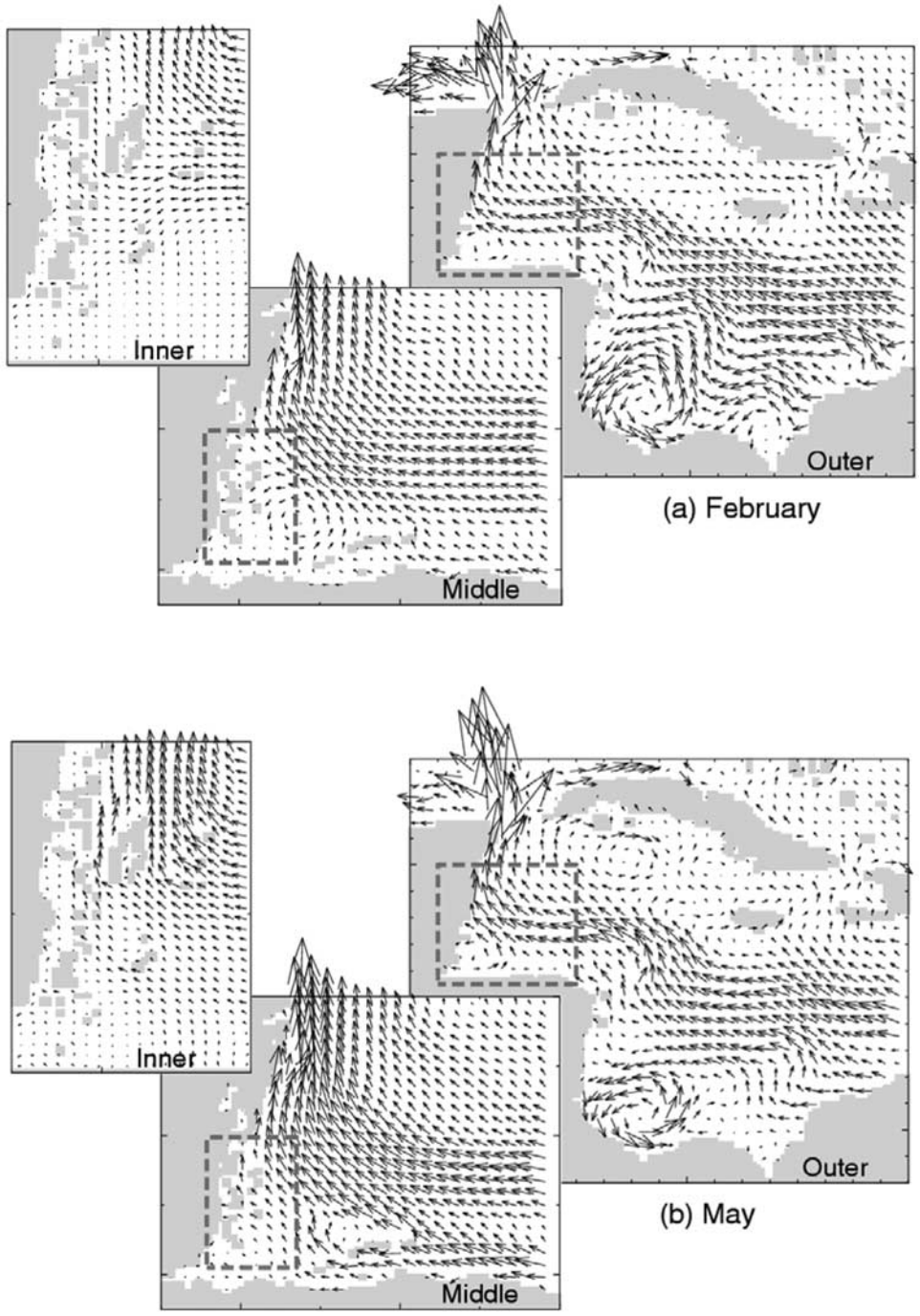

Figure 7. Monthly mean near-surface (5 m) currents in (a) February, (b) May, (c) August, and (d) November calculated from 4-year model results produced by the nested grid system. Velocity vectors are plotted at every third model grid point.

0.40 for those in the southern MBRS (not shown). The *J* value for the middle model results in the southern MBRS is also about 0.40 (Figure 6d). Therefore both the nested grid middle and outer models perform reasonably well in simulating Fratantoni's observed currents in the study region. Comparison of the inner model results with the time-mean observed currents in the BS was not attempted mainly because Fratantoni's data do not resolve the fine-scale circulation features in the BS.

[29] We also calculate the monthly mean, near-surface (5 m) currents in February, May, August, and November (Figure 7) from the 4-year model results. The monthly mean near-surface currents in the WCS produced by the outer model for these four months have large-scale circulation features highly similar to the annual mean, near-surface circulation shown in Figure 6, with significant between month variability. The Caribbean Current is relatively stronger in August and weaker in other three months. The

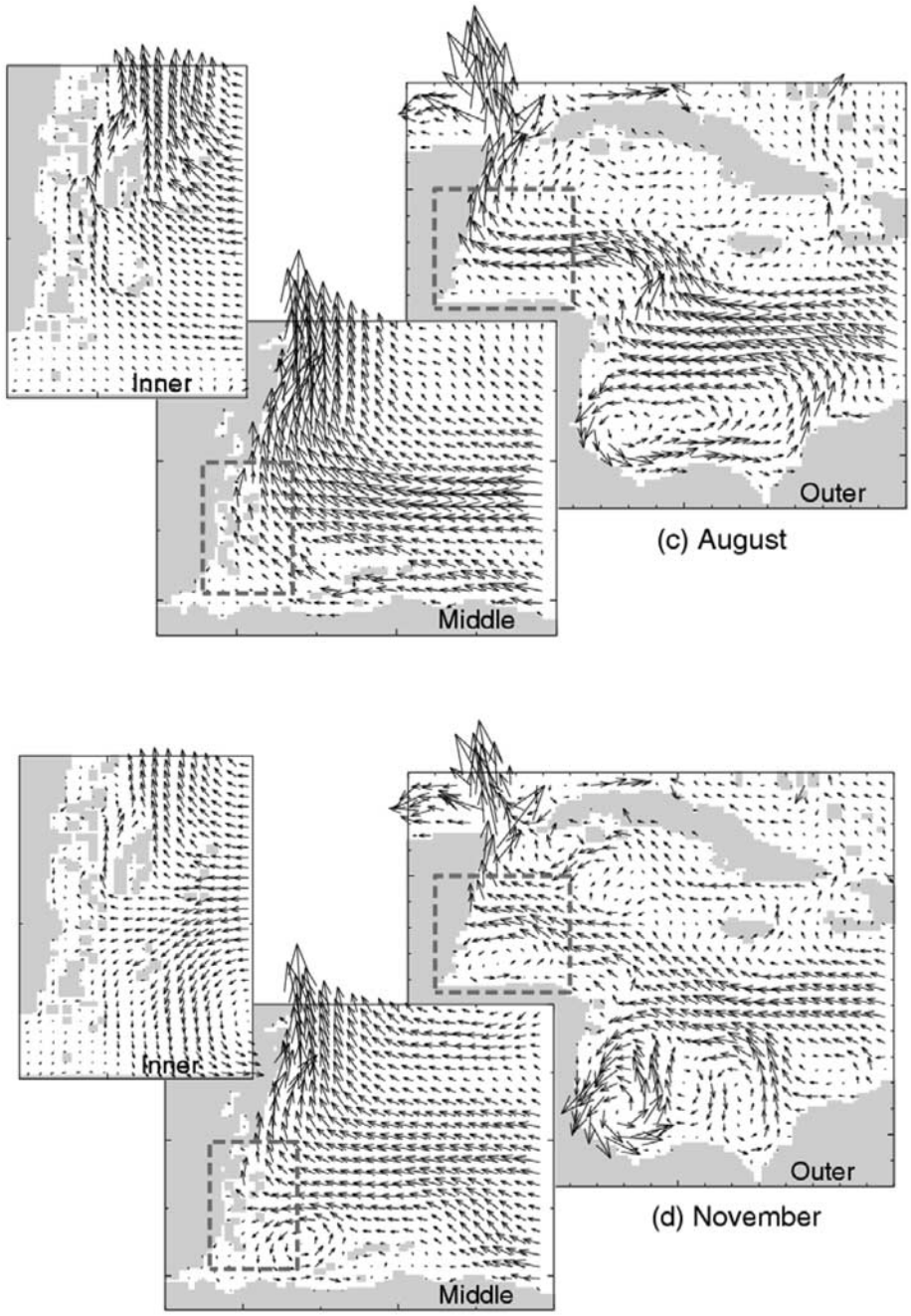

Figure 7. (continued)

Panama-Colombia Gyre is made up of two cyclones in August and November, but only a single cyclone in February and May. The highly variable behaviors of the Panama-Colombia Gyre produced by the nested system are in qualitative agreement with previous findings based on the satellite altimetry data [*Nystuen and Andrade*, 1993; *Andrade and Barton*, 2000] and near-surface drifter data [*Fratantoni*, 2001].

[30] The overall circulation features of the monthly mean near-surface currents over the southern MBRS in the four months produced by the middle model (Figure 7) also compare reasonably well to the annual mean circulation, except that the Caribbean Current in the region is relatively stronger in May and August and weaker in February and November. In addition, there is a small-scale cyclonic recirculation associated with the Honduras Convergence in February and November. This recirculation does not appear, however, in May and August.

[31] The monthly mean near-surface circulation produced by the fine-resolution inner model is characterized by relatively strong and persistent currents in the seaward areas of LRA and TIA, and weak and variable currents in the GOH and adjacent coastal areas of the southern BS (Figure 7). The results are consistent with the annual mean near-surface currents in the same region (Figure 6). The nested grid inner model results also have large month-to-month variability. The monthly mean near-surface currents in the eastern margin of LRA and TIA are relatively weak in

February and November, and stronger in May and August (Figure 7). Over the southern BS, the near-surface currents are relatively weak in February and May, and stronger in August and November. The monthly mean near-surface circulation in February and November produced by the inner model separates into three branches before reaching the southeast margin of TIA: one branch turning northward, a second branch turning southward to form a cyclonic recirculation in the GOH, and a third branch running westward through the passage between TIA and GRA before spreading onto the reef areas within the IC. During May and August, in contrast, the near-surface currents in the southern BS are all approximately northwestward (Figure 7).

3.2. Movements of Near-Surface Particles in Four Reef Areas of the Belizean Shelf

[32] To calculate horizontal movements of near-surface particles in the BS, we set the horizontal velocity vector $\vec{u}$ in equation (6) to be the monthly mean near-surface (5 m) horizontal currents produced by the inner model, and track trajectories of near-surface passive particles numerically using the fourth-order Runge-Kutta scheme [*Press et al.*, 1989], with Δt in equation (7) set to 6 h. Figure 8 displays horizontal distributions of near-surface particles in February, May, August, and November for four clusters of near-surface particles inserted separately in four different reef areas in the BS. (Figure 8 (left) show initial positions of particles inserted in the four areas). The four reef areas are centered at Lighthouse Reef Atoll (LRA), Turneffe Islands Atoll (TIA), Glovers Reef Atoll (GRA) and South Water Cay (SWC), with radii of inserting areas set to about 13, 17, 11, and 15 km, respectively. These four reef areas have been identified as the highest priority areas for biodiversity conservation in the southern MBRS [*Kramer and Kramer*, 2002].

[33] For near-surface particles inserted in the reef area of LRA (particles with the blue color in Figure 8), their horizontal movements during the first 5 days in February and November are similar, characterized by the majority of particles drifting westward onto the eastern margin of TIA, and a small number of particles retaining in the original inserting area around LRA (Figures 8a and 8b). From day 5 to day 10, the near-surface particles in the two months drift further westward into shallow waters east of TIA. By day 15, the particles advected into this region separate approximately into three groups: one group drifting further northward, the second group drifting westward to the south margin of TIA, and the third group retained in the shallow waters east of TIA (Figures 8a and 8d). In May and August, by comparison, most of the near-surface particles inserted initially in the LRA area drift rapidly northwestward during the first 5 days (Figures 8b and 8c), and exit from the northern BS by day 15 in May and by day 10 in August, which is consistent with the fact the monthly mean near-surface currents in the region between TIA and LRA are stronger in May and August than those in other two months (Figure 7).

[34] The horizontal movements of near-surface particles inserted in the TIA reef area (particles with the red color in Figure 8) are functions of their initial positions. Most particles inserted in the central and south lagoons of TIA are retained within the areas for more than 15 days, due mainly to weak near-surface currents in the areas. In February and November, the near-surface particles inserted over the seaward area of TIA are retained in the original inserting area during the first 5 days and then drift gradually northward with the intense near-surface currents. Most particles inserted over the western and northern areas of TIA move northwestward onto the shallow waters of Ambergris Cay (AC) during the first 15 days. In May and August, by comparison, the 15-day movements of near-surface particles inserted in the eastern and western areas of TIA are very similar; characterized by a large number of near-surface particles being advected rapidly northward with the intense, near-surface currents around TIA (Figures 8b and 8c), and a small number of particles remaining in the vicinity of TIA (Figures 8b and 8c).

[35] The near-surface particles inserted in the vicinity of Glovers Reef Atoll (GRA) have two distinct pathways during February (particles with the magenta color in Figure 8a). Particles inserted over the northwestern shallow waters move slowly westward and reach the waters east of SWC by day 15. The majority of particles inserted over the southeastern area are retained there for the duration of the particle tracking, with some particles spreading gradually southeastward. In May, a large number of near-surface particles inserted at the GRA move northwestward, with some of them reaching the northeastern Inner Channel (IC) by day 10 (Figure 8b). In August, the majority of near-surface particles inserted at the GRA area move rapidly northwestward during the first 10 days, and then turn northeastward through the passage between TIA and BBR from day 10 to day 15 (Figure 8c). In November, the near-surface particles inserted at the GRA area drift southwestward during the first 5 days and then turn southeastward afterward (Figure 8d).

[36] The near-surface particles inserted at South Water Cay (SWC) inside of the barrier reef (particles with the green color in Figure 8) experience little horizontal dispersion, with a large number of particles retained in the shallow waters of SWC during the 15-day period. The near-surface particles inserted over the western part of the SWC area drift slowly to the southwestward along the coast of Belize. The particles inserted over the eastern part of the SWC spread gradually southwestward in February and November, and northwestward in May and August.

3.3. Retention and Dispersion of Near-Surface Particles

[37] We calculate the retention index defined in equation (8) on the basis of the horizontal movements of near-surface particles carried by the monthly mean, near-surface (5 m) currents produced by the fine-resolution inner model. The subarea used in the calculation of the retention index is a square box with the horizontal dimension of 80 km by 80 km. A separation distance between centers of two adjacent boxes is set to about 6.6 km to eliminate small-scale features in the results. Within each box, near-surface passive particles are inserted uniformly with 13 particles per 100 km^2 of wet areas. The retention indices of near-surface particles are calculated from the monthly mean near-surface currents in February, May, August, and November (Figure 9). The horizontal distributions of retention indices

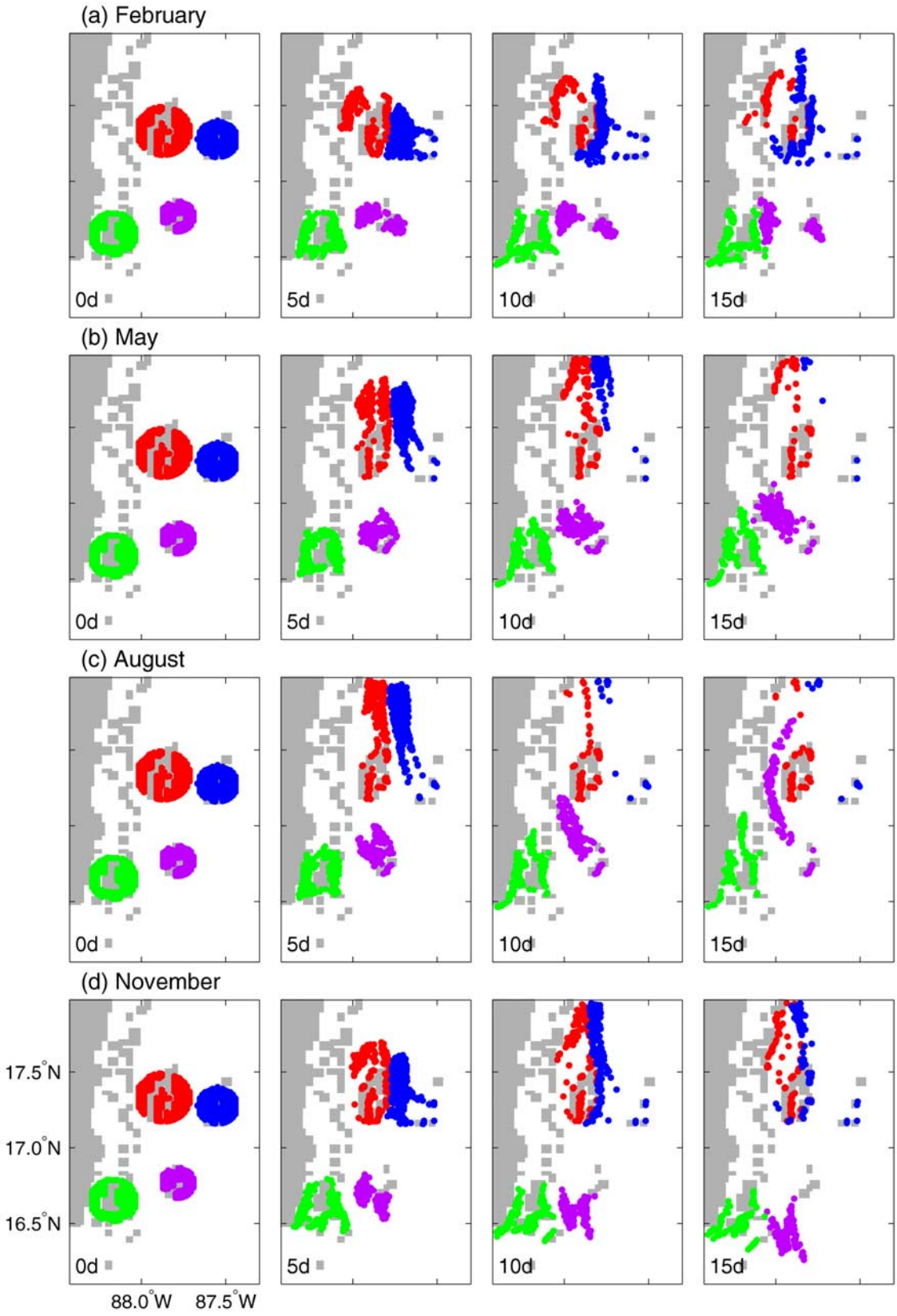

Figure 8. Horizontal positions of near-surface (5 m) particles that are advected passively by monthly mean near-surface currents in (a) February, (b) May, (c) August, and (d) November produced by the nested grid inner model during the 15-day period. The four clusters of particles are seeded over coral reef areas of Lighthouse Reef Atoll (LRA, blue), Turneffe Islands Atoll (TIA, red), Glovers Reef Atoll (GRA, magenta), and South Water Cay (SWC, green), respectively, in the Belizean shelf.

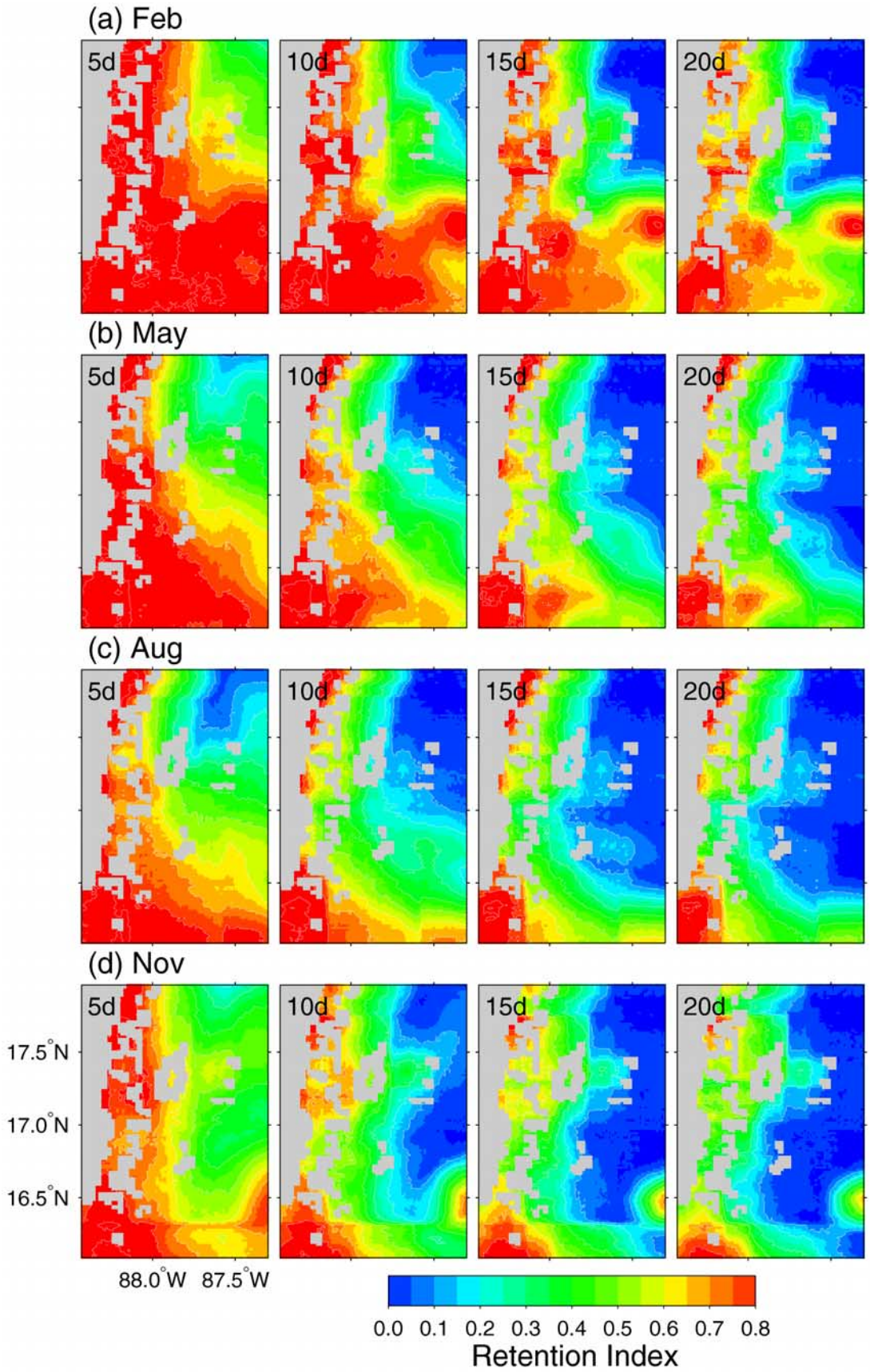

Figure 9. Distributions of retention indices in the Belizean shelf based on the horizontal movements of near-surface particles advected by monthly mean near-surface currents produced by the nested grid inner model in (a) February, (b) May, (c) August, and (d) November. The contour interval is 0.1.

for near-surface particles advected by model currents for five days in each of the four months have similar large-scale features, characterized by relatively high retention indices of about 60–80% over the inner BS between the Belize coast and Belize Barrier Reef (BBR), and lower retention indices of less than 20% over the eastern margins of LRA and TIA. The retention indices for 10 days have similar large-scale horizontal features as those for 5 days, but with reduced magnitudes. The relatively higher retention (or lower dispersion) of near-surface particles over the inner BS, and lower retention (or higher dispersion) of particles over the eastern margins of LRA and TIA are consistent with the general circulation features of the monthly mean currents shown in Figure 7. For particles advected by the monthly mean model currents for 20 days, retention indices are about 40% within most of the Inner Channel and over the Gulf of Honduras, and near zero over the outer BS in the three months other than February.

[38] The calculated retention indices exhibit large month-to-month variability (Figure 9). The retention indices for 20 days of particle movements in the southeastern BS remain high and are about 50% in February, but near zero in the other three months. The result is consistent with the fact that the monthly mean circulation in the region is much weaker in February than that in other three months. In the southern SWC, the retention indices for 20 days are about 70% in February and 50% or less in other three months. Over coastal waters between the Belizean coast and Ambergris Cay, the retention indices for 20 days are about 70% in May and August and about 40% in November.

[39] To further examine the month-to-month variability in retention indices, we calculate area-mean retention indices averaged over four coral reef areas at LRA, TIA, GRA and SWC during a 12 month period. In the LRA area (Figure 10a), the near-surface retention indices for 5 days of particle movements are about 20% in the winter months (December to March), and 5–10% in other months. After 10 days the retention indices in the LRA area reduce to less than 5%, indicating high dispersions due to strong and persistent near-surface currents in the area (Figure 7).

[40] For near-surface particles released in the Turneffe Islands Atoll (TIA) area (Figure 10b), the retention indices for 5 days are about 65% in January and February, and reduce to about 40% in spring (April to June) and summer (July to September). After reaching a minimum value of about 30% in September, the retention indices in the area increase to about 50% in fall (October to December). The retention indices in the TIA area reduce significantly from day 5 to day 10, and reach a constant value after 10 days, which is about 50% in winter, and 40% in other three seasons. The time-invariant retention indices after 10 days can be explained by the fact that a large number of near-surface particles seeded in the central and south lagoons of TIA remain within the lagoons for more than 20 d (Figure 8). For near-surface particles in the Glovers Reef area (GRA) the retention indices for five days are about 50% in winter and early spring and 30–40% from June to August (Figure 10c). After reaching a high value of about 60% in September, the retention indices reduce to 30% in October and December and a minimum value of about 5% in November. After 15 days, the retention indices in the GRA area reduce to about 30% in winter, 15% in spring, summer and later fall, with near zero in October and November.

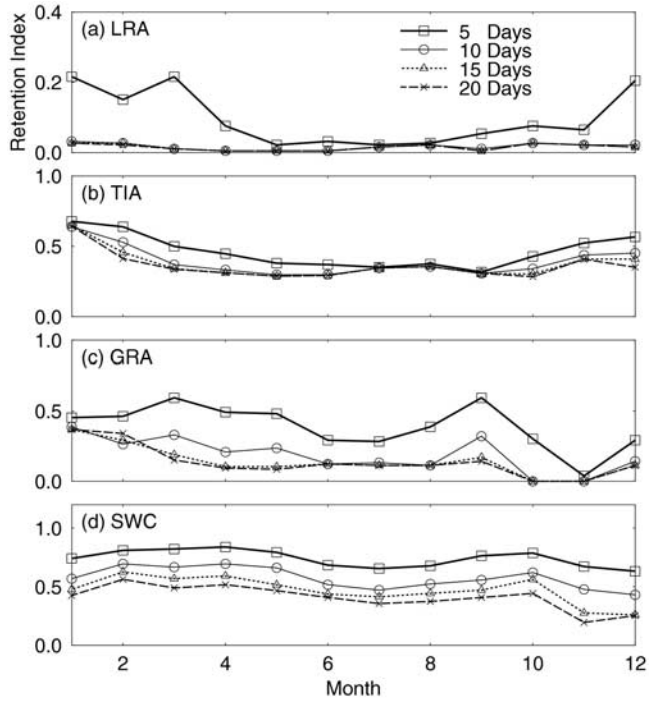

Figure 10. Area mean retention indices for 5, 10, 15, and 20 days of particle movements averaged over reef areas at (a) Lighthouse Reef Atoll (LRA), (b) Turneffe Islands Atoll (TIA), (c) Glovers Reef Atoll (GRA), and (d) South Water Cay (SWC) in the Belizean shelf. The retention indices are calculated on the basis of the horizontal movements of the near-surface particles advected by monthly mean near-surface currents produced by the nested grid inner model.

[41] For near-surface particles inserted in the South Water Cay (SWC) area (Figure 10d), the retention indices for 5 days are high, which are about 80% in winter and early spring, and about 70% from June to September. In fall, the retention indices vary from about 80% in October to about 60% in December. The retention indices in the SWC area reduce continuously with time from day 5 to day 20. For the near-surface particles advected by the model currents for 20 days, the retention indices are about 50% in winter and early spring, 40% in June and summer, 40% in October and 20% in November and December.

3.4. Physical Connectivity of Surface Waters in the Belizean Shelf

[42] To examine hydrodynamic connectivity of surface waters of the Belize shelf, we specify putative source and sink regions associated with each reef area in which particles were inserted (i.e., TIA, GRA) by calculating the upstream and downstream areas of coral reef using the horizontal movements of near-surface particles carried by the monthly mean near-surface (5 m) currents produced by the middle model (Figure 7). We use the intermediate-resolution model results rather than the fine-resolution (inner) model results mainly because the upstream areas of the two atolls extend beyond the domain of the inner model (Figure 11). The upstream area of a given coral reef

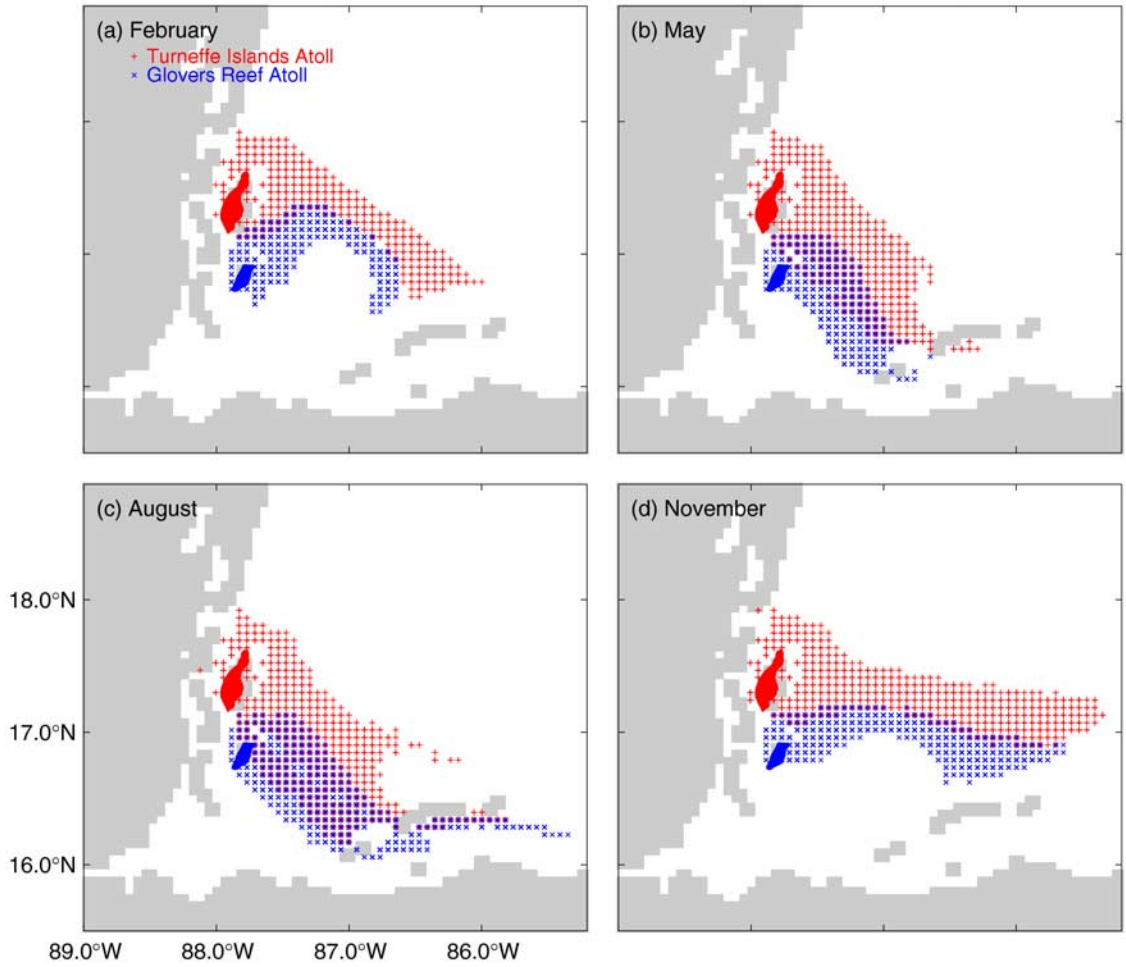

Figure 11. Distributions of upstream areas for coral reefs at Turneffe Islands Atoll (red) and Glovers Reef Atoll (blue) in the Belizean shelf within 30 days calculated from the monthly mean currents produced by the middle model in (a) February, (b) May, (c) August, and (d) November.

in this study is defined as the sum of all subareas from which more than 2% of near-surface particles inserted within each subarea reach the designated sink area within 30 days. Similarly, the downstream area of a given coral reef is defined as the sum of all subareas to which more than 2% of particles originally inserted are advected from the source area within 30 days.

[43] Physically, the upstream area defined above represents a potential area from which the passive particles could be imported to a given reef site within 30 days; and the downstream area is a potential area to which the passive particles could be exported from the given reef site within the same period. We have chosen these criteria to be consistent with those of *Roberts* [1997]. The dimension of the subareas used in the calculation is the same as used in the calculation of retention indices (previous section).

[44] The 30-day upstream area for the Turneffe Islands Atoll (TIA) reef site includes shallow waters of TIA and an offshore corridor connecting deep waters to the southeast margin of TIA with those to the north of the Bay Islands (BI) of Honduras (Figure 11). The horizontal dimension of the offshore corridor is about 200 km by 30 km in February and November and 170 km by 80 km in May and August. Mainly because of a small-scale cyclonic recirculation in the GOH in February and November, the southeastern part of the offshore corridor is located in the deep waters to the north of BI during these two months. In May and August, the southeastern part of the corridor connects the coastal waters off BI, indicating that the near-surface particles released in the coastal waters of BI could affect the TIA reef site within 30 days during this season.

[45] The upstream area of the GRA also includes shallow waters surrounding GRA and an offshore corridor connecting GRA and BI (Figure 11). The offshore corridor in February is a curved shape due to the direct effect of the cyclonic recirculation in the GOH. In May and August, the offshore upstream areas for GRA site are more regular with the horizontal dimension of about 110 km by 50 km, with the southeastern part of the corridor connecting the coastal waters off BI, indicating the strong hydrodynamic connectivity from BI to GRA for passive particles in the surface waters over periods of less than 30 days. In November, the offshore corridor is oriented more east-westward, due again to the effect of the recirculation in the GOH.

[46] The downstream area of the TIA area covers the inner and mid BS between the SWC and AC, with the dimension of about 60 km in the four months (Figure 12). The downstream areas are relatively larger in August and

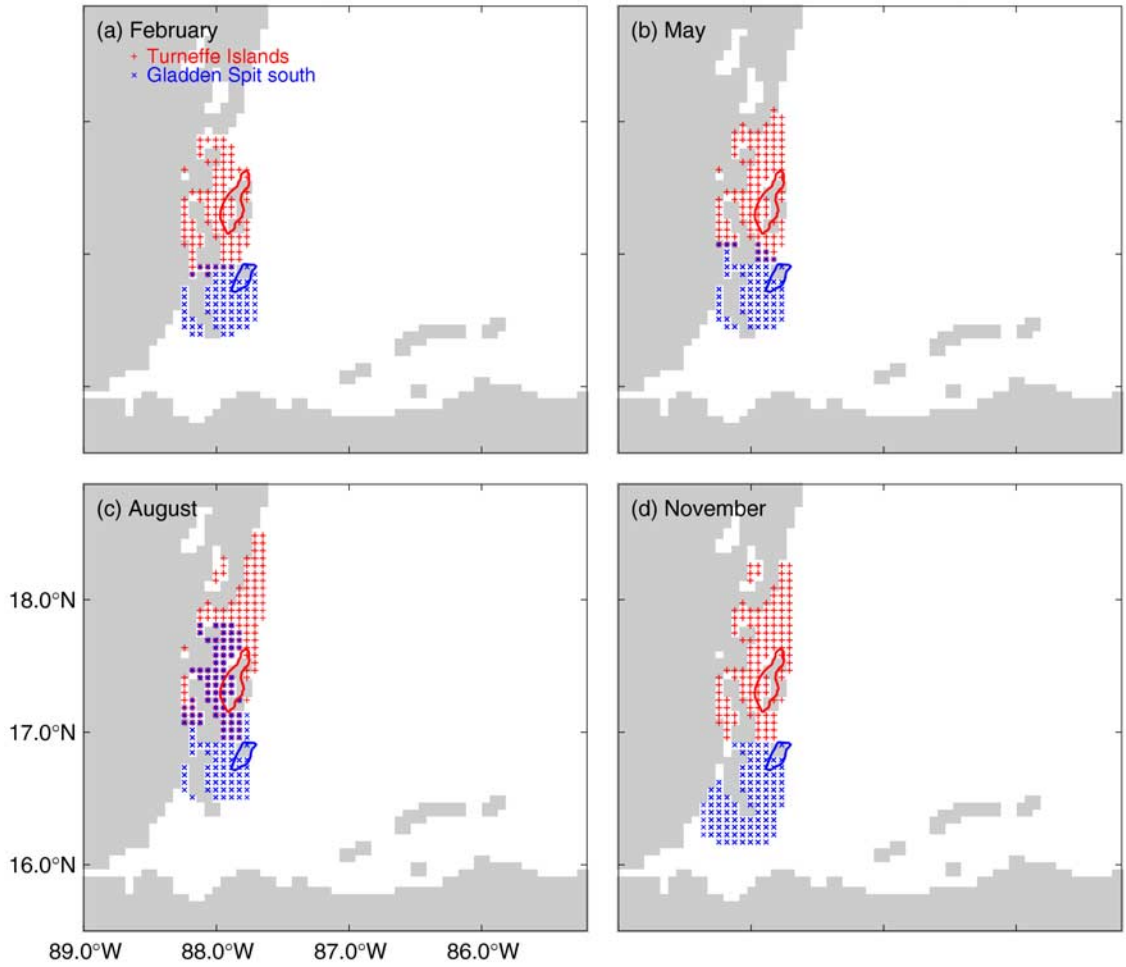

Figure 12. Distributions of downstream areas for coral reefs at Turneffe Islands Atoll (red) and Glovers Reef Atoll (blue) in the Belizean shelf within 30 days calculated from the monthly mean currents produced by the middle model in (a) February, (b) May, (c) August, and (d) November.

smaller in February. The downstream area of the GRA covers the IC in August and more southwestern IC in other three months. Therefore the TIA and GRA reefs are potential sources of particles in the inner BS within 30 days if the particles behave conservatively with respect to the water mass.

4. Summary and Conclusion

[47] Because most species of coral reef fish have a pelagic larval stage lasting for weeks to months, an important issue for the development of ecosystem-based management is the degree of larval exchange among populations of marine organisms inhabiting distinct geographic regions. This flux is difficult to measure directly, but it may be inferred from models of water flow and gene flow, both of which are modified by the behavior of larvae through their capacities to detect and respond to environmental cues and their abilities to orient their vertical and horizontal position by swimming. Our approach in the ECONAR (Ecological Connections Among Reefs) is to first separate this complex interaction into a physical and biological model, and then to recombine them to predict actual dispersion and connectivity, which can be tested using genetic analyses.

[48] This first application of a nested grid, three-dimensional ocean modeling system portrays the hydrodynamic circulation, retention and physical connectivity of surface waters of the Belizean shelf (BS) at spatial and temporal scales relevant to the duration of many larval fish. The novel, two-way nesting technique based on the smoothed, semiprognostic method [*Sheng et al.*, 2005a] exchanges information between subcomponents of the nested model system and specifies the open boundary conditions of the middle and inner models. The main advantage of the nesting technique is that it prevents unrealistic drift of the middle and inner models by adjusting large-scale circulations produced by the two models using the outer and middle model results, respectively, while the model temperature and salinity of the nested system are fully prognostic.

[49] The nested grid system appears to robustly predict the annual and monthly mean circulation in the upper ocean of the WCS, as determined by a comparison of the annual mean currents at 16 m produced by the outer model for the WCS and the middle model for the southern MBRS with the time-mean currents inferred from trajectories of satellite-tracked drifters drogued at 15 m depth in the 1990s [*Fratantoni*, 2001].

[50] The annual mean near-surface circulation in the BS produced by the fine-resolution inner model is characterized by a strong and persistent northwestward flow over the seaward areas of Lighthouse Reef Atoll (LRA) and Turneffe Islands Atoll (TIA), apparently as a direct result of the interaction between the strong, directional Caribbean Current, and weak, spatially variable currents in the southern and inner BS. The monthly mean circulation produced by the nested system also has significant month-to-month variability, with relatively weaker near-surface currents in the shallow waters off LRA and TIA in February and November and stronger in May and August. These patterns reflect variation in the surface wind stress.

[51] We calculated horizontal movements of near-surface particles that are advected passively by the model currents in the BS from the monthly mean near-surface currents produced by the fine-resolution inner model. Within 10 days, most of the near-surface particles inserted initially in the LRA and GRA areas leave the originally seeding areas, while most of the particles seeded initially in the South Water Cay (SWC) and inner BS are retained within the regions. Most of the particles inserted in the central and southern lagoons of ITA are retained in those areas. On the basis of the horizontal movements of near-surface passive particles, we calculated the retention index in the BS, which is defined as the proportion of near-surface particles that are inserted initially in a subarea of 80 km by 80 km remaining within the subarea at later time. Once the retention index R is known, the dispersion rate can be calculated on the basis of $(1 - R)$.

[52] Distributions of retention indices after 15 days indicate that horizontal dispersion of near-surface particles is relatively small in the inner shelf and large in the outer shelf, particularly over the northeastern shelf around the GRA. On the basis of the dispersion indices for four, distinct reef areas over 12 months, the dispersion rate after 15 days is large and more than 90% for the LRA reef, about 85% for the GRA reef, and about 50% for the SWC and TIA reefs.

[53] To allow comparison with the predictions of hydrodynamic connectivity of surface waters in the Caribbean Sea made by *Roberts* [1977], we calculated the upstream and downstream areas of dispersion of passive particles in the MBRS. The 30-day average interaction distances of upstream areas are much larger than those of downstream areas in all seasons. For the regions of TIA and GRA the sources of particle supply are potentially extended to the Bay Islands near the north coast of Honduras, suggesting that the large areas upstream of these two atolls may be important sources of recruits to their fish populations. The downstream areas of TIA and GRA reefs cover mainly the central and southern BS to the west, indicating the potential passive retention of particles in these two regions. Comparisons of these results with those of models incorporating larval fish behavior will provide an indication of the importance of biological processes in determining source-sink relationships among reef fish populations in the MBRS.

[54] **Acknowledgments.** We wish to thank Richard Greatbatch, Barry Ruddick, Pierluigi Pantalone, Leo Oey, Jiuxing Xing, Chris Mooers, and Xiaoming Zhai for their useful suggestions and comments. We thank David Fratantoni for providing the near-surface currents determined from 15-m-drogued satellite-tracked drifters in the North Atlantic and Carsten Eden for providing monthly mean transports in the North Atlantic produced by FLAME. This study was supported by the Collaborative Research Opportunity Program of the NSERC through grant 227965 to P. F. Sale, J. Sheng, and others and by NASA (NNG04GO90G) to USF (subcontract 2500-1083-00-A). J. S. is also supported by the NSERC/MARTEC/MSC Industrial Research Chair.

References

Andrade, C. A., and E. D. Barton (2000), Eddy development and motion in the Caribbean Sea, *J. Geophys. Res.*, *105*, 26,191–26,201.

Andrews, J. H., A. Muller, and L. Bode (1983), Physical oceanography of the Great Barrier Reef, in *Proceedings of the First Great Barrier Reef Conference*, edited by J. T. Baker et al., pp. 89–102, Aust. Inst. of Mar. Sci., Townsville, Queensl., Australia.

Aronson, R., W. Precht, I. Macintyre, and T. Murdoch (2000), Coral bleach-out in Belize, *Nature*, *405*, 36.

Barnier, B., L. Siefridt, and P. Marchesiello (1995), Thermal forcing for a global ocean circulation model using a three year climatology of ECMWF analysis, *J. Mar. Syst.*, *6*, 363–380.

Black, K. P. (1993), The relative importance of local retention and inter-reef dispersal of neutrally buoyant material on coral reefs, *J. Coral Reefs*, *12*, 43–53.

Black, K. P., P. J. Moran, and L. S. Hammond (1991), Numerical models show coral reefs can be self-seeding, *J. Mar. Ecol. Prog. Ser.*, *74*, 1–11.

Carton, J. A., and Y. Chao (1999), Caribbean Sea eddies inferred from TOPEX/Poseidon altimetry and a 1/6° Atlantic Ocean model simulation, *J. Geophys. Res.*, *104*, 7743–7752.

Cesar, H. S. J. (2000), Coral reefs: Their functions, threats and economic value, in *Collected Essays on the Economics of Coral Reefs*, edited by H. S. J. Cesar, pp. 14–39, CORDIO, Kalmar, Sweden.

Cong, L., J. Sheng, and K. T. Thompson (1996), A retrospective study of particle retention on the outer banks of the Scotian Shelf 1956–1993, *Can. Tech. Rep. Hydrogr. Ocean*, *170*, 132 pp.

Cowen, R. K., K. M. M. Lwiza, S. Sponaugle, C. B. Limouzy-Paris, and D. B. Olson (2000), Connectivity of marine populations: Open or closed?, *Science*, *287*, 857–859.

Cowen, R. K., C. B. Paris, D. B. Olson, and J. L. Fortuna (2003), The role of long distance dispersal versus local retention in replenishing marine populations, *J. Gulf Carib. Sci.*, *14*, suppl., 1–10.

da Silva, A. M., C. C. Young, and S. Levitus (1994), *Atlas of Surface Marine Data 1994*, vol. 3, *Anomalies of Heat and Momentum Fluxes*, *NOAA Atlas NESDIS 8*, 413 pp., Dep. of Comm., Washington, D. C.

Davidson, F., R. J. Greatbatch, and B. deYoung (2001), Asymmetry in the response of a stratified coastal embayment to wind forcing, *J. Geophys. Res.*, *106*, 7001–7016.

de Groot, R., M. Wilson, and R. Boumans (2002), A typology for the classification, description and valuation of ecosystem functions, goods and services, *Ecol. Econ.*, *41*, 393–408.

Dengg, J., C. Boening, U. Ernst, R. Redler, and A. Beckmann (1999), Effects of an improved model representation of overflow water on the subpolar North Atlantic, *Int. WOCE Newsl.*, *37*, 10–15.

Dietrich, D. E. (1997), Application of a modified Arakawa 'a' grid ocean model having reduced numerical dispersion to the Gulf of Mexico circulation, *Dyn. Atmos. Oceans*, *27*, 201–217.

Dietrich, D. E., M. G. Marietta, and P. J. Roache (1987), An ocean modeling system with turbulent boundary layers and topography: Numerical description, *Int. J. Numer. Methods Fluids*, *7*, 833–855.

Eden, C., R. J. Greatbatch, and C. W. Boning (2004), Adiabatically correcting an eddy-permitting model of the North Atlantic using large-scale hydrographic data, *J. Phys. Oceanogr.*, *34*, 701–719.

Ezer, T., L.-Y. Oey, and H.-C. Lee (2003), The variability of currents in the Yucatan Channel: Analysis of results from a numerical model, *J. Geophys. Res.*, *108*(C1), 3012, doi:10.1029/2002JC001509.

Fratantoni, D. F. (2001), North Atlantic surface circulation during the 1990's observed with satellite-tracked drifters, *J. Geophys. Res.*, *106*, 22,067–22,093.

Gibson, J., M. McField, and S. Well (1998), Coral reef management in Belize: An approach through integrated coastal zone management, *Ocean Coastal Manage.*, *39*, 229–244.

Greatbatch, R. J., J. Sheng, C. Eden, L. Tang, X. Zhai, and J. Zhao (2004), The semi-prognostic method, *Cont. Shelf Res.*, *24*, 2149–2165.

Haney, R. L. (1971), Surface thermal boundary conditions for ocean circulation models, *J. Phys. Oceanogr.*, *1*, 241–248.

Hannah, C. G., C. E. Naimie, and J. W. Loder (1998), Upper-ocean transport mechanisms from the Gulf of Maine to Georges Bank, with implications for Calanus supply, *Cont. Shelf Res.*, *17*, 1887–1911.

Hatcher, B., et al. (2004), Connecting the dots: Ecological linkages in coral reef ecosystems, paper presented at 10th International Coral Reef Symposium, Int. Soc. for Reef Stud., Naha, Japan.

Hearn, C. J., R. Black, M. S. Johnson, and B. G. Hatcher (2001), Modeling gene currents between coral reef islands, paper presented at 9th International Coral Reef Symposium, Int. Soc. for Reef Stud., Bali, Indonesia.

Hubbell, S. P. (1997), A unifield theory of biogeography and relative species abundance and its application to tropical rain forests and coral reefs, *Coral Reefs*, *16*, S9–S21.

Hughes, T. P., and J. E. Tanner (2000), Recruitment failure, life histories, and long-term decline of Caribbean corals, *Ecology*, *81*, 2250–2263.

Johns, W. E., T. L. Townsend, D. M. Fratantoni, and W. D. Wilson (2002), On the Atlantic inflow to the Caribbean Sea, *Deep Sea Res., Part A*, *49*, 211–243.

Kramer, P. A. and P. R. Kramer (2002), *Ecoregional Conservation Planning for the Mesoamerican Caribbean Reef*, edited by M. McField, 140 pp., World Wildlife Fed., Gland, Switzerland.

Large, W. G., J. C. McWilliams, and S. C. Doney (1994), Oceanic vertical mixing: A review and a model with a nonlocal boundary layer parameterization, *Rev. Geophys.*, *32*, 363–403.

Lawrence, D. R., R. A. Kenchington, and S. Woodley (2002), *The Great Barrier Reef: Finding the Right Balance*, Melbourne Univ. Press, Parkville, Victoria, Australia.

Lu, Y., K. R. Thompson, and D. G. Wright (2001), Tidal currents and mixing in the Gulf of St. Lawrence: An application of the incremental approach to data assimilation, *Can. J. Fish. Aquat. Sci.*, *58*, 723–735.

MacIntyre, I. G., and R. B. Aronson (1997), Field guidebook to the reefs of Belize, in *Proceedings of the 8th International Coral Reef Symposium*, edited by H. A. Lessios and I. G. Macintyre, pp. 203–221, Smithson. Trop. Res. Inst., Balboa, Panama.

Marchesiello, P., J. C. McWilliams, and A. Shchepetkin (2001), Open boundary conditions for long-term integration of regional oceanic models, *Ocean Model.*, *3*, 1–20.

Maul, G. A. (Ed.) (1993), *Climatic Change in the Intra-Americas Sea*, U. N. Environ. Programme, 389 pp., Edward Arnold, London.

Maul, G. A., D. A. Mayer, and S. R. Baig (1985), Comparisons between a continuous 3-year current-meter observation at the sill of the Yucatan Strait, satellite measurements of Gulf Loop Current area, and regional sea level, *J. Geophys. Res.*, *90*, 9089–9096.

Mooers, C. N. K., and G. A. Maul (1998), Intra-Americas Sea circulation, coastal segment (3,W), in *The Sea*, vol. 11, pp. 183–208, John Wiley, Hoboken, N. J.

Murphy, S. J., H. E. Hurburt, and J. J. O'Brien (1999), The connectivity of eddy variability in the Caribbean Sea, the Gulf of Mexico, and the Atlantic Ocean, *J. Geophys. Res.*, *104*, 1431–1453.

Nystuen, J. A., and C. A. Andrade (1993), Tracking mesoscale ocean features in the Caribbean Sea using Geosat altimetry, *J. Geophys. Res.*, *98*, 8389–8394.

Ochoa, J., J. Sheinbaum, J. A. Badan, J. Candela, and D. Wilson (2001), Geostrophy via potential vorticity inversion in the Yucatan Channel, *J. Mar. Res.*, *59*, 725–747.

Oey, L.-Y., and T. Ezer (2004), Modeled and observed empirical orthogonal functions of currents in the Yucatan Channel, Gulf of Mexico, *J. Geophys. Res.*, *109*, C08011, doi:10.1029/2004JC002345.

Orlanski, I. (1976), A simple boundary condition for unbounded hyperbolic flows, *J. Comput. Phys.*, *21*, 251–269.

Palumbi, S. R. (2003), Population genetics, demographic connectivity, and the design of marine reserves, *Ecol. Appl.*, *13*, S146–S158.

Press, W. H., B. P. Flannery, S. A. Teukolsky, and W. T. Vetterling (1989), *Numerical Recipes: The Art of Scientific Computing*, 681 pp., Cambridge Univ. Press, New York.

Purdy, E. G. (1974), Reef configurations: Cause and effect, in *Reefs in Time and Space*, edited by L. F. Laporte, *Spec Publ. Soc. Econ. Paleontol. Mineral.*, *18,* 9–76.

Roberts, C. M. (1997), Connectivity and management of Caribbean coral reefs, *Science*, *278*, 1454–1457.

Sadovy, Y., and A. C. J. Vincent (2002), Ecologic issues and the trades in live reef fishes, *Coral Reef Fishes: Dynamics and Diversity in a Complex Ecosystem*, edited by P. F. Sale, chap. 18, pp. 391–420, Elsevier, New York.

Sheinbaum, J., J. Candela, A. Badan, and J. Ochoa (2002), Flow structure and transport in the Yucatan Channel, *Geophys. Res. Lett.*, *29*(3), 1040, doi:10.1029/2001GL013990.

Sheng, J. (2001), Dynamics of a buoyancy-driven coastal jet: The Gaspe Current, *J. Phys. Oceanogr.*, *31*, 3146–3163.

Sheng, J., and L. Tang (2003), A numerical study of circulation in the western Caribbean Sea, *J. Phys. Oceanogr.*, *33*, 2049–2069.

Sheng, J., and L. Tang (2004), A two-way nested-grid ocean-circulation model for the Meso-American Barrier Reef System, *Ocean Dyn.*, *54*, 232–242.

Sheng, J., and L. Wang (2004), Numerical study of tidal circulation and nonlinear dynamics in Lunenburg Bay, Nova Scotia, *J. Geophys. Res.*, *109*, C10018, doi:10.1029/2004JC002404.

Sheng, J., D. G. Wright, R. J. Greatbatch, and D. E. Dietrich (1998), CANDIE: A new version of the DieCAST ocean circulation model, *J. Atmos. Oceanic*, *Technol.,15*, 1414–1432.

Sheng, J., R. J. Greatbatch, and D. G. Wright (2001), Improving the utility of ocean circulation models through adjustment of the momentum balance, *J. Geophys. Res.*, *106*, 16,711–16,728.

Sheng, J., X. Zhai, and R. J. Greatbatch (2005a), Numerical study of the storm-induced circulation on the Scotian Shelf during Hurricane Juan using a nested-grid ocean model, *Prog. Oceanogr.*, in press.

Sheng, J., R. J. Greatbatch, X. Zhai, and L. Tang (2005b), A new two-way nesting technique based on the smoothed semi-prognostic method, *Ocean Dyn.*, *55*, 162–177, doi:10.101007/s10236-005-0005-6.

Smagorinsky, J. (1963), General circulation experiments with the primitive equation, I. The basic experiment, *Mon. Weather Rev.*, *21*, 99–165.

Smith, R. D., M. E. Maltrud, F. O. Bryan, and M. W. Hecht (2000), Numerical simulation of the North Atlantic Ocean at 1/10°, *J. Phys. Oceanogr.*, *30*, 1532–1561.

Thuburn, J. (1996), Multidimensional flux-limited advection schemes, *J. Comput. Phys.*, *123*, 74–83.

Wilkinson, C. (Ed.) (2004), *Status of Coral Reefs of the World: 2004*, 557 pp., Aust. Inst. of Mar. Sci., Townsville, Queensl., Australia.

Williams, E. H., and L. Bunkley-Williams (2000), Marine major ecological disturbances of the Caribbean, *Infect. Dis. Rev.*, *2*, 110–127.

Wolanski, E., Y. Mazda, K. Furukawa, P. Ridd, J. Kitheka, S. Spagnol, and T. Stieglitz (2001), Water circulation through mangroves and its implications for biodiversity, in *Oceanographic Processes of Coral Reefs: Physical and Biological Links in the Great Barrier Reef*, edited by E. Wolanski, pp. 53–76, CRC Press, Boca Raton, Fla.

B. G. Hatcher and J. Sheng, Department of Oceanography, Dalhousie University, Halifax, NS, Canada B3H 4J1. (jinyu.sheng@dal.ca)

P. F. Sale, Biological Science, University of Windsor, Windsor, ON, Canada N9B 3P4.

L. Tang, Department of Sedimentation Engineering, Institute of Water Resources and Hydropower Research, Beijing, China 100044.